Journal of Solid State Chemistry **146,** 428–436 (1999)
Article ID jssc.1999.8387, available online at http://www.idealibrary.com on IDEAL®

Structure, Thermodynamic, and Magnetic Properties of Ln_4PdO_7 with Ln = La, Nd, Sm, Eu, and Gd

M. Andersson, J. Grins, and M. Nygren[1]

Department of Inorganic Chemistry, Arrhenius Laboratory, Stockholm University, S-106 91 Stockholm, Sweden

Received February 8, 1999; in revised form May 10, 1999; accepted May 21, 1999

The structure of Nd_4PdO_7 has been determined and refined using the Rietveld method and combined Cu$K\alpha_1$ X-ray and neutron powder data in space group $P\bar{1}$ with unit cell $a = 15.972(2)$, $b = 7.1927(7)$, $c = 6.9160(6)$ Å, $\alpha = 96.299(4)$, $\beta = 131.643(3)$, $\gamma = 121.438(3)^\circ$, $V = 353.83(6)$ Å^3 and $Z = 2$, to $R_F = 2.0\%$ (neutron data) and $R_F = 6.2\%$ (X-ray data). The structure is closely related to the monoclinic La_4PdO_7 structure and exhibits Nd atoms coordinated by seven O atoms and Pd atoms coordinated by a square of O atoms. Isolated chains of *trans*-corner-sharing PdO_4 squares are straight in the La_4PdO_7 structure and staggered in the Nd_4PdO_7 structure. Electron and X-ray powder diffraction data show that Ln_4PdO_7 with Ln = Sm, Eu, and Gd is isostructural with Nd_4PdO_7. The enthalpies of dissolution of Ln_4PdO_7 (Ln = La, Nd) in 1.000 M HCl have been measured with an in-house built calorimeter, and from these values the enthalpies of formation for the compounds have been calculated. The decomposition temperatures of Ln_4PdO_7 with Ln = La and Nd in oxygen have been determined by thermogravimetric measurements and found to decrease from 1645 ± 10 K for La_4PdO_7 to 1540 ± 10 K for Nd_4PdO_7. Using these data, an Ellingham diagram has been constructed assuming temperature-independent ΔH_f° and ΔS_f°. The magnetic susceptibilities of Ln_4PdO_7 with Ln = La, Nd, Sm, Eu, Gd, recorded in the temperature range 10–320 K, were found to be in agreement with the expected ones for noninteracting Ln^{3+} ions. © 1999 Academic Press

Key Words: **Ln – Pd oxides; structures; thermodynamic and magnetic properties.**

INTRODUCTION

In a previous article (1) we reported that the compound La_4PdO_7 exhibited a three-way catalytic behaviour, i.e., converted CO, NO, and propene simultaneously to CO_2, N_2, and H_2O after being activated in a slightly reducing atmosphere. The catalytic behavior was ascribed to the formation of nano-sized particles of Pd on the surfaces of micrometer-sized La_2O_3 grains, and it was found that La_4PdO_7 was easily reformed by heat treatment of the reduced material in air. We recently investigated the analogous compounds Ln_4PdO_7 with Ln = Nd, Sm, Eu, and Gd (2, 3) and found that they behave very much like the lanthanum compound, that is, we observed the formation of nano-sized Pd particles on the surface of the Ln_2O_3 grains. The X-ray powder patterns of the Ln_4PdO_7 compounds with Ln = Nd, Sm, Eu, and Gd were similar to that of La_4PdO_7, but they could not be indexed with a similar monoclinic unit cell as that given for La_4PdO_7 (10). We now therefore report the structure of Nd_4PdO_7, determined and refined using the Rietveld method with combined Cu$K\alpha_1$ X-ray and neutron powder data, and present evidence that the Sm-, Eu-, and Gd-analogues are isostructural with Nd_4PdO_7. In this connection it can be noted that Gd_4PdO_7 has never before been reported to form.

Ln_4PdO_7 phases with Ln = La, Nd, Sm, or Eu are known to be thermally very stable in air (4–6), having decomposition temperatures exceeding that of PdO by 285–510 K depending on Ln element. No thermodynamic data are available for these compounds, but such data would be very useful, however, in connection with studies of the reduction/oxidation, i.e., activation/regeneration, processes of these compounds used as exhaust gas catalysts, as well as for the prediction of their thermal stability as a function of the oxygen partial pressure. We have therefore collected enthalpy data for the La and Nd compounds by measurement of their heats of dissolution in 1.000 M HCl, using an in-house built calorimeter; and their decomposition temperatures in oxygen have been determined by thermogravimetric measurements. By combining these data, the Gibbs free energies of formation of the two Ln_4PdO_7 oxides from Ln_2O_3, Pd, and O_2(g) have been calculated as a function of temperature and plotted in an Ellingham diagram. A plot of decomposition temperature vs oxygen pressure has also been constructed for the two compounds.

Finally, we will also present magnetic susceptibility data for the Ln_4PdO_7 compounds with Ln = La, Nd, Sm, Eu, or Gd.

[1]To whom correspondence should be addressed.

0022-4596/99 $30.00

EXPERIMENTAL

The Ln_4PdO_7 compounds with Ln = La, Nd, Sm, Eu, or Gd were synthesized as follows: (i) $PdCl_2$ (p.a. Fluka) and Ln_2O_3 with Ln = Nd, Sm, Eu, and Gd (Ln = Nd, Sm, and Gd 99.9% Johnson Matthey, Eu_2O_3 99.9% Aldrich) or $La(NO_3)\cdot 6H_2O$ (p.a. Merck), respectively, were dissolved in fuming HCl (p.a. Merck) and boiled to dryness; (ii) the residue was slowly heated to 823 K and held at this temperature for one to two hours; (iii) the materials were then ground and heated slowly in air in an oven to 1223–1373 K, depending on the Ln element. After several regrindings and up to 12 days of heat treatment, almost phase pure compounds were obtained, containing typically a few percent of Ln_2O_3 and $Ln_2Pd_2O_5$ as measured by their relative XRPD intensities.

The use of monophasic samples for calorimetric measurements is of great importance, so special care was taken to eliminate $Ln_2Pd_2O_5$ and to minimize and quantify the amounts of Ln_2O_3 present. In the Nd_4PdO_7 case, $Nd_2Pd_2O_5$ was eliminated by reducing Nd_4PdO_7 in a flowing gas mixture of CO/He followed by 161 hours of reoxidation in air (see Ref. 2 for details), whereas just prolonged heat treatment (12 days) yielded an $La_2Pd_2O_5$-free sample in the lanthanum case. The Ln_2O_3 levels present in the samples were estimated by standard additions of Ln_2O_3 to the Ln_4PdO_7 samples, whereby the relative intensities of two strong and nonoverlapping Ln_2O_3/Ln_4PdO_7 peaks were plotted vs the mole fraction of Ln_2O_3 added. The amounts of Ln_2O_3 originally present in the samples were then found by linear extrapolation: the x-axis intercepts corresponded to 4.2 and 3.5 wt% of Ln_2O_3 in the La_4PdO_7 and Nd_4PdO_7 samples, respectively.

The X-ray powder diffraction (XRPD) patterns were recorded with a focusing camera of Guinier–Hägg type, using Cu$K\alpha_1$ radiation and Si as internal standard. The films were evaluated with a film scanner system (7). XRPD data for Rietveld refinements of the structures of Ln_4PdO_7 with Ln = Nd, Sm, and Gd were collected with a STOE STADI/P diffractometer, using Cu$K\alpha_1$ radiation, a sample in symmetrical transmission mode, and a linear position-sensitive detector covering 4.6° in 2θ. Constant wavelength (λ = 1.47 Å) neutron powder diffraction data of Nd_4PdO_7 were collected at the Swedish research reactor R2 in Studsvik. Data were collected between 10° and 128°. The Rietveld structure refinements were made with the GSAS program package (8), which allows several data sets to be used simultaneously.

A JEOL JSM-820 scanning microscope equipped with an energy-dispersive X-ray (EDX) microanalysis system (LINK AN 10000) was used to determine the metal content of the formed compounds. Based on more than 20 EDX point measurements we found that the metal content in all samples was in good agreement with the theoretical Ln/Pd ratio (80/20) required for Ln_4PdO_7.

The decomposition temperatures of the Ln_4PdO_7 compounds with Ln = La and Nd were determined in a thermogravimetric (TG) apparatus (Setaram TAG 24) in oxygen, using a heating rate of 1.25 K/min^{-1}.

Magnetic measurements were carried out in a weak-field ac-susceptometer (Lake Shore 7130) in the temperature range 12–320 K.

An in-house built calorimeter was used for the measurements of the enthalpies of dissolution of Ln_4PdO_7 with Ln = La and Nd. It consisted of a 10-cm^3 plastic container which was filled with 5.00 cm^3 of 1.000 M HCl and placed inside a plastic-foam insulation block. The solution was stirred at 250 rpm by means of a magnetic stirrer, and its temperature was monitored by a Cu-constantan thermocouple mounted inside a small glycerol-filled glass tube placed in contact with the solution. An ice/water bath was used as cold junction. The temperature was first allowed to stabilize and was then recorded every second, using a computer and the program Quadstar (Balzers). After about 100 s of recording, a weighed and well-ground amount of the sample to be dissolved was introduced into the container by means of a 1.0 cm^3 disposable syringe with cut-off top, into which the powder had been placed. After 5000 s the data collection was aborted. The obtained data, see Fig. 1a, were corrected for nonadiabatic conditions in the following way: first, the times for the onset of heat evolution (t_{add}) and the maximum temperature were established, and the time difference between them multiplied by 2.5 (named t_{25} below) was taken as the maximum time needed for full dissolution of the sample in question. The validity of this assumption was checked for all samples by stopping subsequent experiments just before t_{25}, followed by centrifugation and weighing of

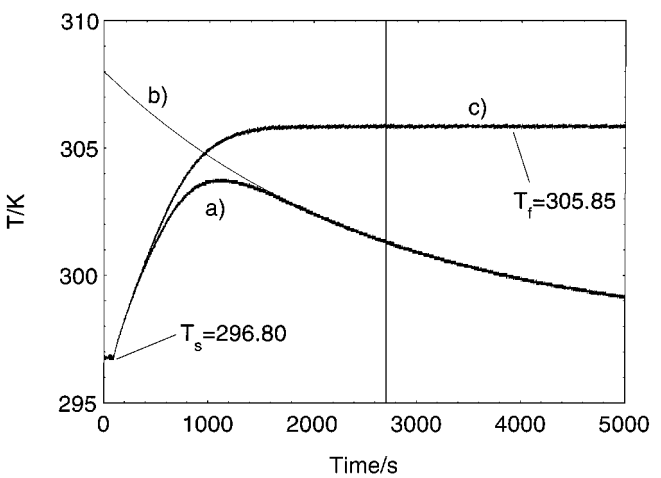

FIG. 1. Temperature vs time plot for dissolution of Nd_4PdO_7 in 1.000 M HCl showing (a) the original curve, (b) a curve fitted to the cooling branch of the original curve, and (c) the calculated adiabatic curve. T_s and T_f correspond to the starting and final temperature used for thermodynamic calculations, and the vertical line denotes $t = t_c = t_{add} + t_{25}$, the constants being defined in the text.

the undissolved material (if any). In all cases the undissolved amount was less than 2 wt% of the amount added.

Well beyond the completion of the chemical reaction, the heat flow is proportional to the time derivative of the temperature dT/dt and, since the former (Newton's law of cooling) is proportional to the temperature difference $T - T_0$ (T = internal temperature, T_0 = external), the differential equation [1] holds.

$$dT/dt = -C\cdot(T - T_0) \qquad [1]$$

The reaction was assumed to be completed at $t_{add} + t_{25} = t_c$ and from this point Eq. [1] can be integrated in the form

$$T(t) = (T_c - T_0)\cdot\exp[-C\cdot(t - t_c)] + T_0, \qquad [2]$$

where T_c corresponds to the temperature observed at the time t_c. By fitting data recorded from t_c forward into Eq. [2] one obtains the coefficients C and T_0. Subsequently, the adiabatic temperatures $T_{adi,i}$ (i.e., temperatures in absence of heat loss) can be obtained, point by point, by adding to the first temperature point to be compensated T_1 the value $\Delta T_1 = C(T_1 - T_0)\Delta t$ ($\Delta t = 1$ s), to the next temperature point T_2 the value $\Delta T_1 + C(T_2 - T_0)\Delta t, \ldots$, to the temperature point T_n the value $\Delta T_1 + \cdots \Delta T_{n-1} + C(T_n - T_0)\Delta t$. One obtains (see Fig. 1c) a diagram with a plateau value T_f, which corresponds to the final adiabatic temperature. The first point to be compensated, T_1,was the first measurement with $T \geq T_0$ or in cases with T_0 being somewhat less than the starting temperature the compensation was started when T was 0.1° higher than the starting temperature.

The starting temperature T_s (calculated as the average temperature 20 s before the addition of the sample) was subtracted from the final adiabatic temperature T_f (see Fig. 1), and this temperature difference was divided by the amount of dissolved material to yield the temperature rise per mole, which is proportional to the molar enthalpy of dissolution. Compensation for the undissolved fraction of material was performed, as well as a correction for the Ln_2O_3 content of the Ln_4PdO_7 samples. Typical values of the constants discussed above are (values taken from Fig. 1): $T_s = 296.80$ K, $T_f = 305.85$ K, $T_c = 301.31$ K, $T_0 = 297.61$ K, $C = 3.812 \times 10^{-4}$ s^{-1}, $t_{25} = 2593$ s, and $t_{add} = 102$ s.

To test the accuracy of the calorimeter, different oxides (MgO p.a. Merck, Y_2O_3 grade fine HCST, Ln_2O_3 with Ln = La, Nd, and Gd as above) were dissolved, and the obtained molar enthalpies of dissolution (ΔH_{dis}) were compared to each other. Nd_2O_3 was used as calibration compound, and it was assumed that the dissolution yields hydrated metal ions and H_2O(l). The ΔH_{dis} values are presented in Table 1 togheter with the corresponding literature values (9) and the obtained t_{25} values. It is obvious from Table 1 that our in-house built calorimeter yields quite accurate ΔH_{dis} values, but the data indicate that the dissolution characteristics (t_{25}) of the samples could affect the results, as materials that dissolve more slowly tend to give somewhat higher values of ΔH_{dis}.

TABLE 1
Measured Molar Enthalpies of Dissolution (ΔH°_{dis}) for Selected Oxides and their Corresponding Literature Values (9)

Oxide	Measured ΔH°_{dis} (kJ/mol^{-1})	Literature value for ΔH°_{dis} (kJ/mol^{-1})	Deviation from literature value (%)	t_{25} (min)[a]
Nd_2O_3	Reference	− 442.2	—	4.0
MgO	− 155.2	− 151.5	− 2.5	3.0
La_2O_3	− 487.5	− 478.1	− 2.0	3.3
Y_2O_3	− 390.7	− 399.2	+ 2.2	46.3
Gd_2O_3	− 396.8	− 413.8	+ 4.2	47.6

Note. Nd_2O_3 has been used as calibration compound.
[a] Defined in the text.

RESULTS AND DISCUSSION

Powder Diffraction

The Guinier–Hägg XRPD patterns for Ln_4PdO_7 with Ln = La, Nd, Sm, Eu, Gd are shown in Fig. 2 for the 2θ-range 26–33.5°. The pattern for the La compound was found to agree well with the reported structure and monoclinic unit cell of La_4PdO_7 ($a = 13.469(1)$, $b = 4.0262(1)$, $c = 9.448(1)$ Å, $\beta = 133.42(1)°$ (10)), while those for the other Ln compounds, although similar, could not be indexed on the basis of this type of cell. They could, however, be indexed with C-centered triclinic cells of similar dimensions but with

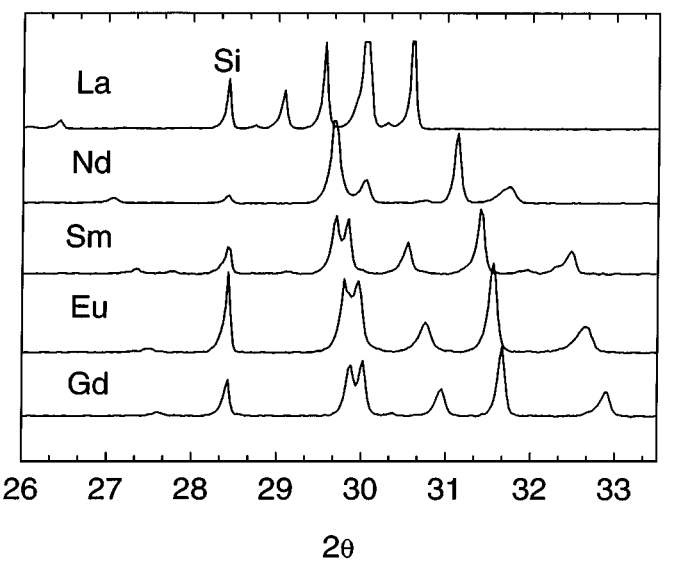

FIG. 2. Guinier–Hägg patterns of Ln_4PdO_7 with Ln = La–Gd. Si was added as an internal standard.

slightly obtuse α and γ angles, e.g., for Nd_4PdO_7 $a = 13.186(2)$, $b = 3.9701(6)$, $c = 9.426(1)$ Å, $\alpha = 91.761(8)$, $\beta = 133.843(3)$, $\gamma = 91.20(1)^\circ$. A triclinic cell of this kind would imply a direct lowering of the space group symmetry from $C2/m$ for La_4PdO_7 to $C\bar{1}$ ($P\bar{1}$) for the other compounds.

Electron diffraction patterns of Nd_4PdO_7 were, however, not compatible with the triclinic cell above. They could instead be accounted for by a primitive triclinic cell which is approximately related to the monoclinic La_4PdO_7 cell by;

$$\mathbf{a}_{tri} = -1/2\cdot\mathbf{a}_{mon} - 3/2\cdot\mathbf{b}_{mon} + \mathbf{c}_{mon}$$

$$\mathbf{b}_{tri} = -1/2\cdot\mathbf{a}_{mon} + 1/2\cdot\mathbf{b}_{mon} - \mathbf{c}_{mon}$$

$$\mathbf{c}_{tri} = 1/2\cdot\mathbf{a}_{mon} - 1/2\cdot\mathbf{b}_{mon}.$$

This type of triclinic cell was subsequently verified by electron diffraction to be valid also for Sm_4PdO_7 and Gd_4PdO_7. It thus contains the same number of Ln_4PdO_7 formula units as the monoclinic C-centered cell of La_4PdO_7 but is primitive triclinic.

Unit cell parameters were ultimately determined by Rietveld refinements, based on Guinier–Hägg data with Si as internal standard and using atomic coordinates derived from neutron and/or X-ray diffractometer data (see below). They are given in Table 2. The estimated standard deviations (esd) in these are probably underrated by factors 2.5–3, since serial correlation (11) in the refinements was not accounted for. For comparison, the indexed Guinier–Hägg powder pattern of Gd_4PdO_7 is listed in Table 3, up to the 20th observed line. The indexed pattern yielded the unit cell parameters $a = 15.80(3)$, $b = 7.12(1)$, $c = 6.795(8)$ Å, $\alpha = 95.7(1)^\circ$, $\beta = 131.25(7)^\circ$, $\gamma = 122.8(1)^\circ$, $V = 334.3$ Å^3 and the cell figure-of-merit $M_{20} = 25$. These cell parameters agree well within error with those obtained from the Rietveld refinement, but they have notably higher esd. The unit cells used are not reduced. Corresponding reduced cells are obtained by the transformation of axes $\mathbf{a}_r = \mathbf{c}$, $\mathbf{b}_r = -\mathbf{b}$, $\mathbf{c}_r = \mathbf{a} + \mathbf{b} + 2\cdot\mathbf{c}$, yielding e.g. in the case of Nd_4PdO_7 a reduced unit cell $a = 6.916$, $b = 7.193$, $c = 7.930$ Å, $\alpha = 70.44^\circ$, $\beta = 72.16^\circ$, $\gamma = 83.70^\circ$.

The variation of the unit cell parameters of the Ln_4PdO_7 compounds with the Shannon–Prewitt (eight-coordinated) ionic radius of the Ln^{3+} ions (12) is shown in Fig. 3. The unit cell volumes follow Vegard's law well.

TABLE 2
Unit Cell Parameters for Ln_4PdO_7

	La	Nd	Sm	Eu	Gd
a (Å)	16.080	15.972(2)	15.905(2)	15.833(1)	15.795(1)
b (Å)	7.1556	7.1927(7)	7.1678(7)	7.1350(6)	7.1142(5)
c (Å)	7.0289	6.9160(6)	6.8541(7)	6.8138(6)	6.7853(5)
α (°)	96.475	96.299(4)	95.969(4)	95.886(3)	95.723(2)
β (°)	132.894	131.643(3)	131.358(3)	131.279(2)	131.241(2)
γ (°)	119.163	121.438(3)	122.342(3)	122.496(3)	122.771(2)
V (Å^3)	372.14	353.83(6)	343.16(6)	338.10(5)	333.50(4)

Note. The triclinic cell parameters for La_4PdO_7 are converted from the true monoclinic cell given in Ref. (10).

TABLE 3
Powder X-Ray Diffraction Pattern of Gd_4PdO_7

hkl	$2\theta_{obs}$	$\Delta 2\theta$	d_{obs} (Å)	I/I_0 (%)
$\bar{1}10$	13.313	0.003	6.65	2
$1\bar{1}1$	24.119	0.015	3.687	2
200	25.626	−0.004	3.473	7
$\bar{2}20$	26.807	0.004	3.231	1
$\bar{4}02$	27.655	0.007	3.223	9
$2\bar{2}1$	29.904	−0.010	2.986	75
$\bar{4}21$	30.047	0.001	2.972	82
$0\bar{2}1$	30.407	−0.004	2.937	6
$3\bar{1}2$	30.985	0.006	2.884	51
$\bar{2}02/$	31.701	0.001	2.821	100
$\bar{5}11$		−0.019		
$\bar{4}01$	32.744	0.008	2.733	5
110	32.940	−0.001	2.717	46
101	37.080	0.011	2.423	3
$3\bar{1}1$	38.919	−0.004	2.3122	1
$\bar{2}\bar{2}2$	39.182	0.003	2.2973	3
$1\bar{3}1$	43.347	0.009	2.0857	15
020	43.692	0.007	2.0701	4
$\bar{7}13$	44.070	0.008	2.0532	30
$\bar{5}\bar{1}3$	44.443	−0.009	2.0368	4
$\bar{2}\bar{2}3$	45.634	−0.006	1.9864	10

Note. $\Delta 2\theta = 2\theta_{obs} - 2\theta_{calc}$. $\lambda = 1.5406$ Å.

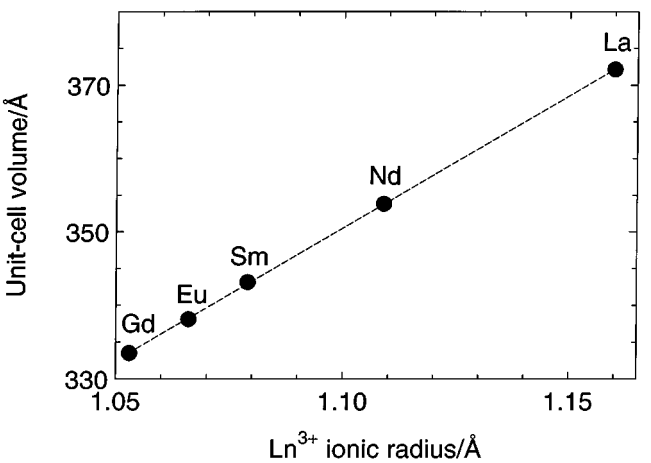

FIG. 3. Unit-cell volume for Ln_4PdO_7, Ln = La–Gd, vs the ionic radius of the Ln^{3+} ion.

Refinement of the Structure of Nd_4PdO_7 Using X-Ray and Neutron Powder Data

The atomic coordinates for La_4PdO_7 (10) were transformed to the triclinic cell and used as a starting set. The structure was refined using simultaneously the X-ray ($2\theta = 10$–$80°$, with 428 reflections) and neutron data ($2\theta = 10$–$85°$, with 552 reflections). Different starting configurations were tested to ensure a global minimum in the refinements. The calculations converged if structural and profile-fitting parameters were refined in succession. The largest correlation coefficient for positional parameters was 0.89, observed between the x and z coordinates for O1. The backgrounds were fitted by 15 Chebyshev polynomial coefficients and the X-ray reflection profiles modeled by a pseudo-Voigt function (13) with 7 coefficients. A Debye–Scherrer absorption correction was applied for the neutron data. The 2θ scales for the two data sets were adjusted to each other by refining the neutron wavelength and the cell parameters. The secondary phases Nd_2O_3 (14) and $Nd_2Pd_2O_5$, with atomic coordinates taken from $La_2Pd_2O_5$ (15), were included with collective thermal parameters, lattice parameters, and phase fractions refined. A total of 82 variables were used in the final refinement, including 33 positional parameters and 3 collective thermal parameters for the Nd, Pd, and O atoms in Nd_4PdO_7. The obtained atomic coordinates are given in Table 4 and selected bond distances and angles are given in Table 5. The fit between observed and calculated patterns for the X-ray and neutron data is illustrated in Figs. 4 and 5, respectively. The corresponding refinement indices are $wR_p = 0.037$, $R_p = 0.028$, $D\text{wd} = 1.18$, $R_F = 0.020$ for the neutron data and $wR_p = 0.035$, $R_p = 0.023$, $D\text{wd} = 0.49$, $R_F = 0.062$ for the X-ray data, and with a total $\chi^2 = 1.55$. The refined phase fractions of Nd_2O_3 and $Nd_2Pd_2O_5$ were 3.8 and 4.6%, respectively, in the sample used for neutron diffraction and 1.9 and 2.2%, respectively, in the X-ray case.

Electron diffraction patterns indicate that the Ln_4PdO_7 phases with Ln = Sm or Gd are isostructural with Nd_4PdO_7, and given the XRPD findings above we feel confident in that the Eu compound also has this structure. But reliable refinements of the structures of Sm_4PdO_7 and Gd_4PdO_7 could not be obtained from X-ray powder diffractometer recordings, particularly so with respect to the positions of the O atoms, due to the relatively large number of positional parameters, 33, to refine. The derived structure for Nd_4PdO_7 is, however, seen to be close to *C*-centered

TABLE 4
Structural Parameters Refined from X-Ray and Neutron Powder Diffraction Data for Nd_4PdO_7

Atom	Site	x	y	z	U_{iso} (Å^2)
Nd1	2*i*	0.7785(15)	0.1563(23)	0.7811(30)	0.008(1)
Nd2	2*i*	0.2820(15)	0.6830(21)	0.7737(29)	0.008(1)
Nd3	2*i*	0.1421(11)	0.0074(18)	0.6413(22)	0.008(1)
Nd4	2*i*	0.6237(13)	0.4545(19)	0.5885(24)	0.008(1)
Pd1	1*a*	0	0	0	0.008(3)
Pd2	1*e*	1/2	1/2	0	0.008(3)
O1	2*i*	0.104(3)	0.681(4)	0.349(5)	0.011(1)
O2	2*i*	0.602(2)	0.148(3)	0.360(5)	0.011(1)
O3	2*i*	0.174(2)	0.419(3)	0.880(5)	0.011(1)
O4	2*i*	0.694(2)	0.027(3)	0.969(5)	0.011(1)
O5	2*i*	0.921(2)	0.056(3)	0.114(4)	0.011(1)
O6	2*i*	0.479(2)	0.560(4)	0.259(5)	0.011(1)
O7	2*i*	0.258(2)	0.319(3)	0.564(5)	0.011(1)

Note. Triclinic, $a = 15.972(2)$, $b = 7.1927(7)$, $c = 6.9160(6)$ Å, $\alpha = 96.299(4)°$, $\beta = 131.643(3)°$, $\gamma = 121.438(3)°$, $Z = 2$, $P-1$.

TABLE 5
Atomic Distances (Å) and Angles (°) in Nd_4PdO_7

Nd1–O2	2.31(2)	Nd2–O4	2.27(2)
O4	2.38(2)	O2	2.32(2)
O1	2.41(2)	O1	2.36(2)
O1	2.43(2)	O3	2.39(2)
O5	2.47(2)	O2	2.44(2)
O6	2.56(2)	O7	2.54(2)
O3	3.02(2)	O5	2.79(2)
O7	3.47(2)	O6	3.39(2)
Nd3–O3	2.27(2)	Nd4–O2	2.27(2)
O4	2.37(2)	O3	2.28(2)
O1	2.41(2)	O4	2.31(2)
O7	2.44(2)	O6	2.45(2)
O5	2.46(2)	O6	2.51(2)
O6	2.53(2)	O5	2.58(2)
O3	2.82(2)	O7	2.68(2)
O5	3.22(2)	O4	3.74(2)
Pd1–O5 2×	2.04(2)	Pd2–O7 2×	2.04(2)
O7 2×	2.07(2)	O6 2×	2.07(2)
O5–Pd1–O7	87.4(6)	O6–Pd2–O7	85.8(7)
Pd1–O7–Pd2	150.4(9)		

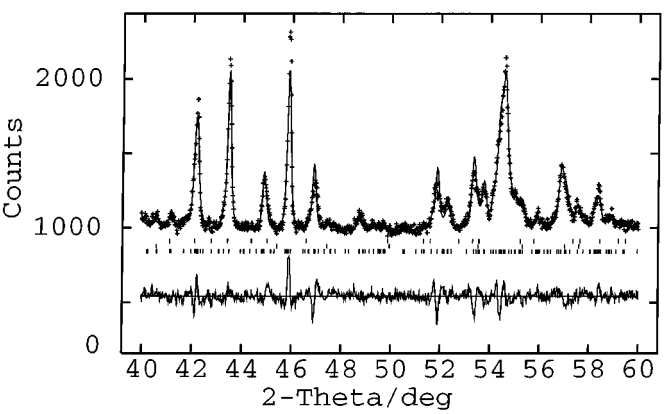

FIG. 4. Observed (crosses), calculated, and residual XRPD patterns for Nd_4PdO_7 in the 2θ range 39–61°.

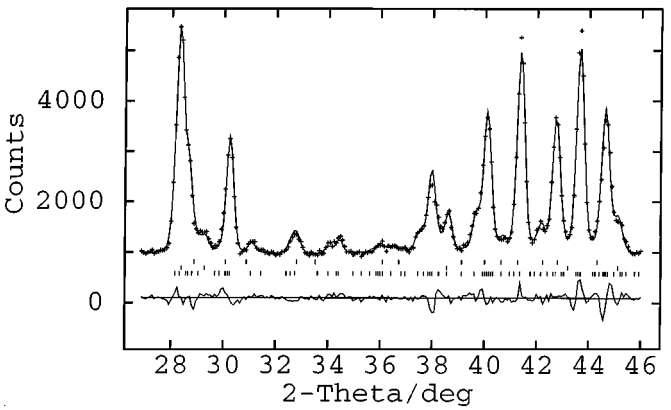

FIG. 5. Observed (crosses), calculated, and residual neutron powder diffraction patterns for Nd_4PdO_7 in the 2θ range 26–47°.

(cf. Table 4), and simplified structure models for Sm_4PdO_7 and Gd_4PdO_7 could accordingly be refined in space group $C\bar{1}$. The corresponding residual indices were for Sm_4PdO_7 $wR_p = 0.022$, $R_p = 0.017$, $Dwd = 0.91$, $R_F = 0.062$, $\chi^2 = 1.34$, and for Gd_4PdO_7 $wR_p = 0.021$, $R_p = 0.016$, $Dwd = 0.91$, $R_F = 0.061$, and $\chi^2 = 1.18$. It should be stressed, however, that the electron diffraction patterns clearly show that the cell is not C-centered; furthermore, such a symmetry is not compatible with the staggered chains of PdO_4 squares found in the Nd_4PdO_7 structure.

Description of the Nd_4PdO_7 Structure

The crystal chemistry of La–Pd oxides, and their structural relationship with the A- and B-type Ln_2O_3 structures, has been admirably described by Attfield and Férey (15). The La–Pd oxides form a series of structures that are in their idealized form built up from a primitive cubic lattice of oxide ions in which Pd^{2+} and Ln^{3+} ions are found at the face and body centers of the O_8 cubes and thus satisfy the requirements of both a square planar coordination for Pd^{2+} and a high coordination number, ideally 8, for the Ln^{3+} ions. The structure of La_4PdO_7 is monoclinic with symmetry $C2/m$ (10), while that of Nd_4PdO_7 exhibits a triclinic distortion of this structure type, with symmetry $P\bar{1}$. Perspective views of corresponding layers in the structures of Nd_4PdO_7 and La_4PdO_7 are shown in Fig. 6. A major difference between the structures is that the chains of PdO_4 squares are straight in the latter structure and staggered in the former, with Pd–O–Pd angles of 150.4(9)°. The observed decrease in lattice symmetry from monoclinic for Ln_4PdO_7 with Ln = La to triclinic for Ln = Nd (and Sm, Eu, Gd) is directly related to the staggering of these chains. The triclinic cell used here for the latter compounds, $\mathbf{P}_{tri}$, may be described by an equivalent triclinic cell, $\mathbf{P}'_{tri}$, by the transformation $\mathbf{a}'_{tri} = \mathbf{c}_{tri}$, $\mathbf{b}'_{tri} = -\mathbf{a}_{tri} - \mathbf{b}_{tri}$, $\mathbf{c}'_{tri} = -\mathbf{b}_{tri} - \mathbf{c}_{tri}$. This transformed cell is in turn related to a smaller primitive triclinic cell, $\mathbf{P}''_{tri}$, which describes the lattice of La_4PdO_7 if its symmetry is directly lowered from $C2/m$ to $P\bar{1}$ ($\mathbf{a}''_{tri} = 1/2 \cdot \mathbf{a}_{mon} - 1/2 \cdot \mathbf{b}_{mon}$, $\mathbf{b}''_{tri} = 1/2 \cdot \mathbf{a}_{mon} + 1/2 \cdot \mathbf{b}_{mon}$, $\mathbf{c}''_{tri} = \mathbf{c}_{mon}$) by $\mathbf{a}'_{tri} = \mathbf{a}''_{tri}$, $\mathbf{b}'_{tri} = 2 \cdot \mathbf{b}''_{tri}$, $\mathbf{c}'_{tri} = \mathbf{c}''_{tri}$. If, however, the chains of PdO_4 squares are staggered, half of the inversion centra present in the monoclinic cell, and thus also in the $\mathbf{P}''_{tri}$ cell, are absent, together with the mirror plane and twofold symmetry axis, and the unit cell volume is doubled, e.g., by a doubling of the $\mathbf{b}''_{tri}$ axis.

The triclinic distortion of the Ln_4PdO_7 structures with Ln = Nd, Sm, Eu, Gd can be understood as an adaption to shorten the average Ln–O distances while retaining the dimensions of the planar PdO_4 groups. The monoclinic La_4PdO_7 structure cannot, e.g, contract in the b axis direction without causing a decrease of the Pd–O distances, but the triclinic distortion provides the possibility of a more isotropic decrease of the unit cell dimensions with only minor alterations of the square PdO_4 units.

Assignment of coordination numbers for the rare-earth atoms is ambiguous for the structures of both La_4PdO_7 and Nd_4PdO_7. In the La_4PdO_7 structure the two crystallo-

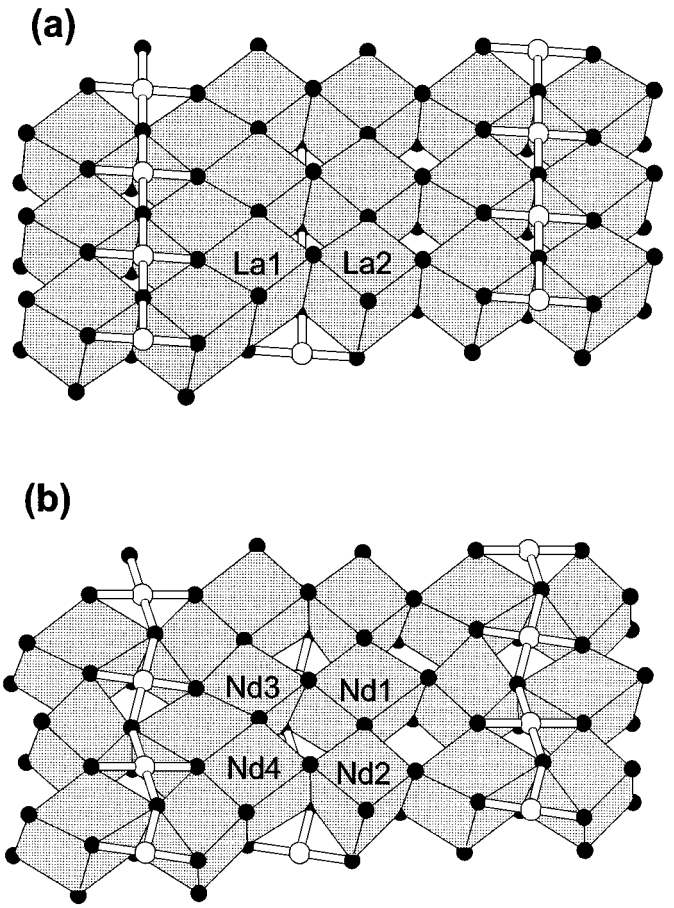

FIG. 6. Perspective views of corresponding layers in the structures of (a) La_4PdO_7 and (b) Nd_4PdO_7, parallel to the planes $(\bar{4}0\bar{3})$ and $(\bar{2}4\bar{1})$, respectively.

TABLE 6
Enthalpy of Dissolution of Ln_4PdO_7 with Ln = La and Nd

Compound	ΔH°_{dis} (kJ/mol^{-1})	t_{25} (min)
La_4PdO_7	-974 ± 6	5.6
Nd_4PdO_7	-907 ± 23	44.2

graphically different La atoms have 7 and 8 O atoms, respectively, at distances 2.36–3.01 Å, with an average La–O distance of 2.56 ± 0.21 Å. In the Nd_4PdO_7 structure the four different Nd atoms all have 7 O atoms at distances 2.27–3.02 Å, with an average of 2.47 ± 0.18 Å.

Calorimetric and Thermogravimetric Measurements

The obtained values of dissolution enthalpy (ΔH°_{dis}) for the Ln_4PdO_7 oxides are presented in Table 6 together with the corresponding t_{25} values. To minimize systematic errors, calibration substances with t_{25} values as close as possible to those of the Ln_4PdO_7 oxides were chosen, i.e., Nd_2O_3 in the La_4PdO_7 case and Gd_2O_3 in the case of Nd_4PdO_7, see also Tables 1 and 6.

The following reaction was assumed to describe the dissolution of Ln_4PdO_7

$$Ln_4PdO_7(s) + 14H^+(aq) + 4Cl^-(aq) \rightarrow 4Ln^{3+}(aq) + PdCl_4^{2-}(aq) + 7H_2O(l) \quad [3]$$

The enthalpies of formation of Ln_4PdO_7 with Ln = La and Nd were calculated using available values (9) for enthalpy of formation of the involved ions and $H_2O(l)$. The obtained ΔH°_f values are listed in Table 7. (ΔH_f for $PdCl_4^{2-}$ used in the calculations was calculated from Ref. 16, using ΔH_f data for Cl^- and Pd^{2+} from Ref. 9.)

In order to be able to calculate the ΔS°_f values for these Ln_4PdO_7 oxides, we determined the decomposition temperatures in oxygen of these oxides, see Table 7, by means of a TG unit. The XRPD patterns of the decomposed materials matched those of Ln_2O_3 and Pd, with some additional weak reflections matching $La(OH)_3$ for Ln = La. (DTA runs were also performed to verify that no phase transitions occurred in the interval from room temperature up to the decomposition temperature of the Ln_4PdO_7 oxides.) Because ΔG° for the decomposition reaction

$$Ln_4PdO_7(s) \rightarrow 2Ln_2O_3(s) + Pd(s) + 0.5O_2(g) \quad [4]$$

must be zero at the decomposition temperature, and ΔH° for the reaction can be calculated using ΔH°_f-values for Ln_2O_3 from Ref. (9); assuming that the enthalpy of formation (ΔH°_f) of Ln_4PdO_7 is temperature independent, ΔS° of reaction [4] can be calculated from the relation $\Delta G^\circ = \Delta H^\circ - T\Delta S^\circ$. Since ΔS°_f values are available (9) for Ln_2O_3, ΔS°_f values for Ln_4PdO_7 could be calculated, and the obtained results are given in Table 7.

Using the enthalpies and entropies of formation thus obtained for the Ln_4PdO_7 compounds, together with literature data (see below), an Ellingham diagram (Fig. 7) was constructed to visualize the redox chemistry of the oxides. ΔG°_f values for Ln_2O_3 were calculated from room temperature up to the decomposition temperature of the corresponding Ln_4PdO_7 compound, using the computer program "HSC Chemistry" (9), and the obtained values were used together with our data given above for Ln_4PdO_7 to construct the lines denoted a and b in Fig. 7. The c and d lines in the diagram were directly obtained by plotting calculated ΔG° values (9) of the indicated reaction vs the temperature.

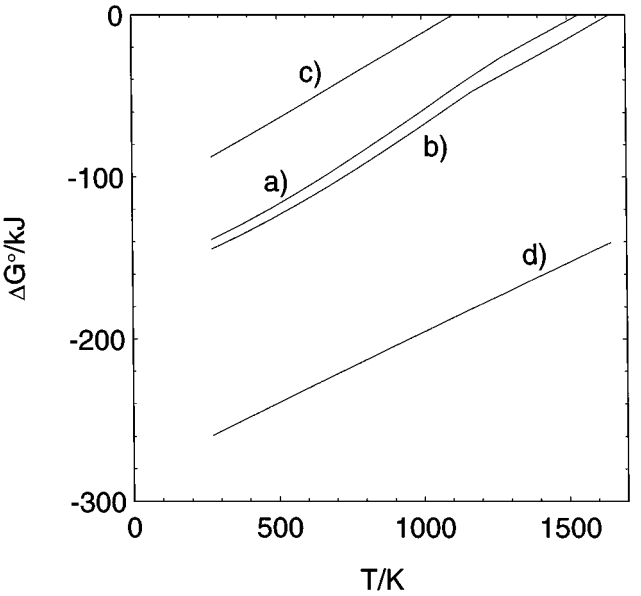

FIG. 7. Ellingham diagram showing the Gibbs free energy (ΔG°) for the following reactions as a function of temperature: (a) $2Nd_2O_3(s) + Pd(s) + 0.5O_2(g) \rightarrow Nd_4PdO_7(s)$; (b) $2La_2O_3(s) + Pd(s) + 0.5O_2(g) \rightarrow La_4PdO_7(s)$; (c) $Pd(s) + 0.5O_2(g) \rightarrow PdO(s)$; (d) $CO(g) + 0.5O_2(g) \rightarrow CO_2(g)$.

TABLE 7
Calculated Enthalpy and Entropy of Formation, ΔH°_f and ΔS°_f, and Decomposition Temperature, T_{dec}, of Ln_4PdO_7 with Ln = La and Nd

Compound	ΔH°_f (kJ/mol^{-1})	ΔS°_f (J/mol^{-1}K^{-1})	T_{dec} (K)
La_4PdO_7	-3755 ± 7	-672	1645 ± 10
Nd_4PdO_7	-3778 ± 24	-670	1540 ± 10

Note. The errors in ΔS°_f can be calculated by dividing the ΔH°_f errors by T_{dec}.

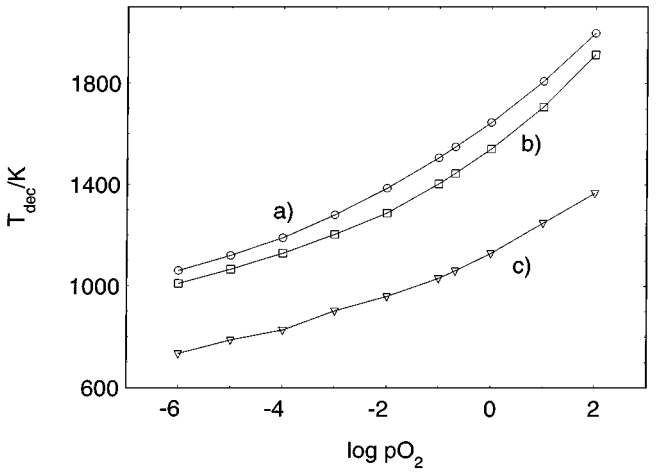

FIG. 8. Plot showing calculated decomposition temperatures for (a) La_4PdO_7, (b) Nd_4PdO_7, and (c) PdO as a function of oxygen partial pressure.

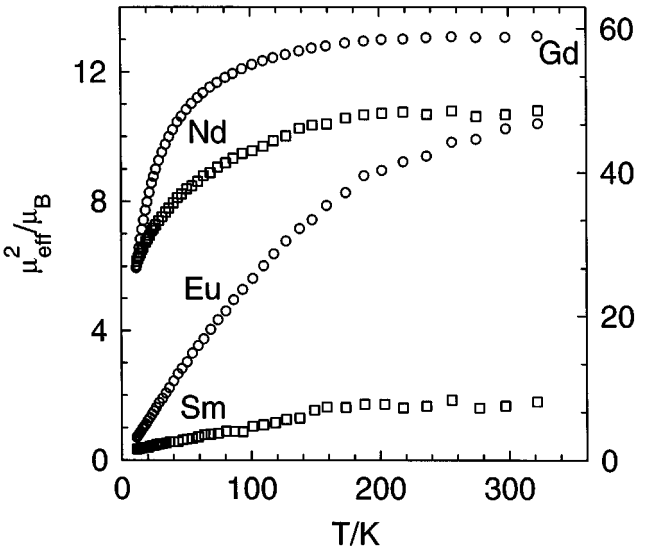

FIG. 9. The square of the effective number of Bohr magnetons as a function of temperature for Ln_4PdO_7 with Ln = Nd, Sm, Eu (left vertical axis) and Gd (right vertical axis).

Using the thermodynamic data given above, it is also possible to predict the decomposition temperatures of Ln_4PdO_7 as a function of oxygen pressure, using

$$T_{dec} = (2\Delta H^\circ_{f,Ln_2O_3} - \Delta H^\circ_{f,Ln_4PdO_7})/(2\Delta S^\circ_{f,Ln_2O_3} - \Delta S^\circ_{f,Ln_4PdO_7} - R\ln(pO_2^{1/2})) \quad [5]$$

and the ΔH°_f and ΔS°_f values of Ln_2O_3 with Ln = La and Nd given in Ref. 9. The calculated decomposition temperatures of these two Ln_4PdO_7 oxides at selected oxygen pressures are presented in Fig. 8 together with the corresponding figures for PdO for comparison.

From the Ellingham diagram given in Fig. 7 it can be seen that the Ln_4PdO_7 compounds with Ln = La and Nd are more stable than $2La_2O_3$ + PdO at all temperatures, and our calculations show that this stabilization is clearly an enthalpy effect in the La case, whereas in the Nd case it is more difficult to make such a definite statement. It is also evident from the Ellingham diagram that reduction of these Ln_4PdO_7 compounds to Pd and Ln_2O_3 is possible at all temperatures using carbon monoxide as the reducing agent. However, in a previous article (3) we have shown that reduction of La_4PdO_7 and Nd_4PdO_7 with CO does not take place until at about 812 and 848 K, respectively, and we ascribe this to the decomposition reaction being kinetically retarded.

Magnetic Susceptibility

La_4PdO_7 was observed to be diamagnetic in the temperature range investigated (10–320 K), and to have a susceptibility of the order of -1.6×10^{-9} m^3/mol^{-1}. The Pd atoms thus do not give rise to any temperature-dependent paramagnetic signal. Figure 9 shows the square of the measured effective number of Bohr magnetons, μ^2_{eff}, as a function of temperature for Ln_4PdO_7 with Ln = Nd, Sm, Eu, and Gd. Corrections for diamagnetism and sample holder were applied to these data, but were found to be negligible. The temperature dependencies of μ^2_{eff} are qualitatively those expected for noninteracting Ln^{3+} ions (17), e.g., calculated using Van Vleck's equation and accounting for contributions from excited states. Expected and observed μ_{eff} values at room temperature are for Nd 3.3, 3.5, for Sm 1.5, 1.4, for Eu 3.5, 3.3, and for Gd 7.9, 7.7, respectively. Thus the data show no indications of any significant magnetic interactions between the rare-earth atoms in the compounds.

ACKNOWLEDGMENTS

The authors thank Mr. H. Rundlöf (Studsvik) for the collection of neutron diffraction data and Prof. L. Kihlborg for recording the electron diffraction patterns. This work has been financially supported by the Swedish Research Council for Engineering Sciences.

REFERENCES

1. M. Andersson, K. Jansson, and M. Nygren, *Catalysis Letters* **39,** 253 (1996).
2. M. Andersson, K. Jansson, and M. Nygren, *Thermochimica Acta* **318,** 83 (1998).
3. M. Andersson, K. Jansson, and M. Nygren, *J. Mater. Chem.* **9,** 265 (1999).
4. C. L. McDaniel and S. J. Schneider, *J. Res. Nat. Bur. Stand., Phys. Chem.* **72A** (1), 27 (1968).
5. B. G. Kakhan, V. B. Lazarev, and I. S. Shaplygin, *Russ. J. Inorg. Chem.* **27** (8), 1180 (1982).

6. B. G. Kakhan, V. B. Lazarev, and I. S. Shaplygin, *Russ. J. Inorg. Chem.* **27** (9), 1352 (1982).
7. K. E. Johansson, T. Palm, and P-E. Werner, *J. Phys.* **13,** 1289 (1980).
8. A. C. Larson, and R. B. Von Dreele, Los Alamos National Laboratory Report No. LA-UR-86-748 (1987).
9. "HSC Chemistry," computer program by A. Roine, Outokumpu Research Oy., Pori, Finland.
10. J. P. Attfield, *Acta Crystallogr., Sect. B* **44,** 563 (1988).
11. J.-F. Berár and P. Lelann, *J. Appl. Crystallogr.* **24,** 1 (1991).
12. R. D. Shannon, *Acta Crystallogr., Sect. A* **32,** 751 (1976).
13. P. Thompson, D. E. Cox, and J. B. Hastings, *J. Appl. Crystallogr.* **20,** 79 (1987).
14. J. X. Boucherle, *Acta Crystallogr., Sect. B* **31,** 2745 (1975).
15. P. Attfield, and G. Férey, *J. Solid State Chem.* **80,** 286 (1989).
16. T. Ryhl, *Acta Chem. Scand.* **26** (7), 2961 (1972).
17. M. M. Schieber, "Experimental Magnetochemistry." North-Holland, Amsterdam, 1967.